Available online at www.sciencedirect.com
ScienceDirect
Journal of Catalysis 243 (2006) 395–403
JOURNAL OF CATALYSIS
www.elsevier.com/locate/jcat

Preparation of nanostructured nitrogen-containing carbon catalysts for the oxygen reduction reaction from SiO_2- and MgO-supported metal particles

Paul H. Matter, Eugenia Wang, Umit S. Ozkan *

Department of Chemical Engineering, The Ohio State University, Columbus, OH 43210, USA

Received 28 May 2006; revised 30 July 2006; accepted 31 July 2006

Abstract

Nitrogen-containing carbon was prepared from the vapor deposition of acetonitrile at 900 °C over silica- or magnesia-supported Fe, Co, and Ni particles. The byproducts of pyrolysis were monitored by mass spectrometry. The carbon formed from silica precursors was washed with KOH to remove the silica and HCl to remove metal particles, whereas the carbon formed from magnesia samples was washed with HCl to remove the support and the metal. The solid carbon product was characterized with N_2 physisorption to measure surface area and pore volume distribution, X-ray diffraction to determine the crystalline phases present, and temperature- programmed oxidation to determine ash and nitrogen content. Magnesia was more readily removed from the carbon compared with silica. A significant amount of metal, encased in carbon, remained in the samples after washing. The Co particles led to a higher content of bulk nitrogen in the carbon, as high as 2.9% based on oxidation measurements. Electron microscopy imaging confirmed that all of the metal particles catalyzed the formation of various types of carbon nanofibers, with the diameter and structure of the fibers varying with different metal–support precursor combinations. A possible application for these fibers is oxygen reduction reaction catalysts for proton-exchange membrane fuel cell cathodes.

Keywords: Nitrogen-doped carbon; CN_x; Carbon nanofibers

1. Introduction

With the emergence of nanotechnology, carbon may prove to be one of the most useful materials over the next several decades. Emerging potential applications for nanostructured carbon include water purification, electronics, sensors, polymer composites, hydrogen storage, catalysis, and electrodes. The reason for the broad range of applications for carbon is the unique properties that it can have depending on its structure at the molecular and nanoscale levels.

Doping carbon nanostructures adds another dimension to these structures' properties. For example, carbon atoms within a graphite matrix can be replaced with similar elements, such as boron or nitrogen, during graphitization. In a semiconductor sense, this could be considered *p* or *n* doping (for B or N, respectively). Boron is electron-deficient and is known to improve the ability of a graphite matrix to accept electrons, whereas nitrogen has an extra electron that improves electron donation [1]. Likewise, doping of carbon can affect such properties as pH, catalytic activity, conductivity, and nanostructure [2]. In addition, surface functional groups can result from the doping process, which changes the carbon's characteristics. Such changes have many implications for potential applications, especially electrodes and catalysis. Previous research by our group has found that nitrogen-doped carbon nanostructures could potentially replace platinum in PEM fuel cell cathodes [3–5]. Other potential uses for doped carbon could include solid base catalysts [6], sensor materials [7,8], and lithium ion battery electrodes [9–12].

Although several processes exist for the preparation of carbon nanostructures, the most common technique is catalytic chemical vapor deposition (CCVD). This technique is considered the easiest for large-scale production of nanostructured carbon [13]. In such a process, a hydrocarbon atmosphere is heated in the presence of a metal catalyst to temperatures typically between 500 and 1200 °C. The metal particle can be supported, unsupported, or "floated" into the reaction zone in

* Corresponding author.
E-mail address: ozkan.1@osu.edu (U.S. Ozkan).

0021-9517/$ – see front matter
doi:10.1016/j.jcat.2006.07.029

the form of a volatile organometallic compound. Preparation of doped carbon can be as simple as adding the appropriate nitrogen or boron species to the feed in the carbon preparation procedures described previously. For instance, decomposition of C/N mixtures including acetonitrile [14–18], pyridine [14,19–21], and larger nitrogen-containing organic molecules [21–23] over metal particles can produce nitrogen-doped nanofibers. Generally, in the systems studied to date, unsupported metal particles were used as catalysts for nanofiber growth. Other potential routes for doped nanofiber preparation include the pyrolysis of organic macrocycles, such as phthalocyanine, that contain metal centers [7,24], and the pyrolysis of polymers containing nitrogen or boron [25]. Typically, the nitrogen content of the fibers formed from pyrolytic methods is on the order of 5%, although this can vary depending on the feed composition and the treatment temperature [18,22,26].

Previously, we have reported the growth of nitrogen-containing carbon (CN_x) fibers from acetonitrile using metal particles (Fe or Ni) supported by carbon [3] or alumina [4,5]. These fibers were found to have high activity for the oxygen reduction reaction in an acid electrolyte. In the current study, we examine the growth of nitrogen-doped carbon nanofibers from metal particles (Fe, Co, or Ni) supported by SiO_2 or MgO. The metal particles chosen are known to be effective catalysts for nanofiber formation from hydrocarbon sources [13,27], and varying the metal particle used for fiber growth is well known to affect the carbon structure [27–31]. The supports chosen are attractive for fiber growth, because silica and magnesia can be separated from carbon using KOH or HCl washes, respectively, which are much more benign than the HF wash used to dissolve alumina studied previously [4,5]. Furthermore, the effect of the support for the metal particles could influence the structure of the carbon that forms, as has been observed for the growth of carbon nanofibers from Ni particles on various supports [32]. Physical characterization of the fibers is also presented using an array of techniques to determine the effectiveness of the wash, and characterize the solid carbon that forms during the CCVD. The majority of characterization is carried out on fibers that have gone through the washing process, since removing the support purifies the active component for the ORR reaction, and makes characterization of the carbon material easier. The next paper in this series will present the surface and electrochemical properties of the fibers and their activity for the oxygen reduction reaction.

2. Experimental

2.1. Fiber preparation

Nitrogen-containing carbon fibers were prepared from SiO_2- or MgO-supported Ni, Co, or Fe. The silicon oxide high-surface area catalyst support (215 m^2/g, from Alfa Aesar) was used without further treatment. Two types of MgO supports were used, one with a surface area of 55 m^2/g used as received from Leco Co. and the other, a type of MgO "nanopowder" with a surface area of 150 m^2/g used as received from Sigma–Aldrich. The supports were impregnated by the incipient wetness method with an aqueous solution of the metal acetate salt. A concentration of the acetate solution was chosen to provide a final metal loading of 2 wt% (unless noted otherwise), and the total volume of water used was equivalent to the total volume of the support pores. The precursor was dried at 100 °C overnight. TGA was used to determine the weight loss incurred during temperature ramping in an inert atmosphere up to 900 °C, to accurately determine the carbon yield during the acetonitrile treatment. A total of 2 g of precursor was used for fiber growth. The precursor was placed in a 6-inch quartz boat inside a quartz tube furnace, and the temperature was ramped to the treatment value (550 or 900 °C) at 10 °C/min under N_2 flow at 150 sccm. For treatment temperatures of 550 °C, the metal salt was reduced in situ with 5% H_2 in N_2 before flowing acetonitrile over the precursor, whereas at 900 °C, the salt was simply allowed to be reduced by the acetonitrile. The acetonitrile treatments lasted 2 h, using nitrogen flowing at 150 sccm saturated with acetonitrile ($P_{vap} = 72.8$ mm Hg at 25 °C) by means of a room-temperature bubbler. After the treatment, the temperature was lowered to room temperature under N_2 flow overnight.

2.2. Fiber purification

Fibers prepared using silica-based supports were purified by subsequent KOH and HCl washes. The product from the acetonitrile treatment was refluxed in 1 M KOH for 6 h, then washed with distilled water by suction filtration. Next, the material was refluxed in 1 M HCl for 6 h, then washed with distilled water by suction filtration. The recovered fibers were dried overnight at 100 °C. In one case, for comparison, a fiber sample was washed with HF acid using a procedure described elsewhere [4,5].

Fibers prepared using magnesia-based supports were purified using only an HCl wash. The product from the acetonitrile treatment was refluxed in 1 M HCl and then washed with distilled water by suction filtration. The recovered fibers were dried overnight at 100 °C.

2.3. Temperature-programmed acetonitrile pyrolysis (TPAP)

Analysis of the byproducts of acetonitrile pyrolysis was performed with an on-line Cirrus mass spectrometer (MS). For these experiments, 100 mg of catalyst precursor was placed loosely (with a channel to prevent plugging) in a quartz tube and placed horizontally in a furnace with an on-line mass spectrometer to analyze the exit stream. The temperature was ramped from room temperature to 900 °C at a rate of 10 °C/min while flowing He (20 sccm) saturated at room temperature with acetonitrile. The MS scanned for ions between 1 and 100 AMU.

2.4. BET surface area and pore size distribution

Surface area measurements were done by N_2 physisorption using both a Micromeritics ASAP 2010 and a Micromeritics Accusorb 2100E. The BJH pore size distributions were obtained from the desorption isotherm of N_2 physisorption experiments with the Micromeritics ASAP 2010.

2.5. X-ray diffraction

X-ray diffraction (XRD) patterns were obtained with a Bruker D8 diffractometer using Cu$K\alpha$ radiation. Samples were supported by polyethylene holders with a 0.5-mm-deep reservoir for the powder samples. Patterns were recorded between 10° and 90° 2Θ.

2.6. Temperature-programmed oxidation

Temperature-programmed oxidation (TPO) of samples was carried out using a Setaram TG-DSC 111 with the product stream being analyzed by a Cirrus mass spectrometer. Approximately 10 mg of sample was loaded into the thermogravimetric analyzer, and the temperature was ramped at 5 °C/min to 750 °C in 10% O_2 in He flowing at 60 sccm (split evenly between the reference and sample side). Both the TG and DSC signals were recorded. The mass spectrometer was used to follow oxides of nitrogen and carbon that formed from the combustion; all ions between 1 and 100 AMU were recorded. Products were quantified using ionization probabilities provided by the manufacturer.

2.7. Transmission electron microscopy

Transmission electron microscopy (TEM) was performed with a Philips Tecnai TF20. Samples were supported by laceyformvar carbon, which was supported by a 200-mesh copper grid. The carbon samples were dispersed with excess ethanol before being deposited on the grid. Distributions of fiber diameters and structures were obtained from 50 different, randomly chosen fibers.

3. Results and discussion

3.1. TPAP

Before reporting information about the solid carbon product that forms during pyrolysis treatments, we describe the gaseous products of the pyrolysis treatments. TPAP pyrolysis byproducts were analyzed using an on-line mass spectrometer. As an example, Fig. 1 shows the products released during TPAP analysis for pure silica. During the temperature ramp, some oxygenated gases (mainly CO_2 and water) were released from the surface of all samples. For silica, a sharp CO_2 peak was observed just above 800 °C. Although reduction of the supports could not be confirmed or denied (as was the case for alumina [5]), removal of oxygen from the support again seemed to precede consumption of acetonitrile for the silica and magnesia samples. Addition of metal to the support led to even more CO_2 production well below 900 °C, due to the presence of additional oxygen in the acetate salt (data for metal-doped supports not shown).

After the furnace temperature reached 900 °C, there was little difference in the products produced over the range of supports tested. The main byproducts produced were hydrogen

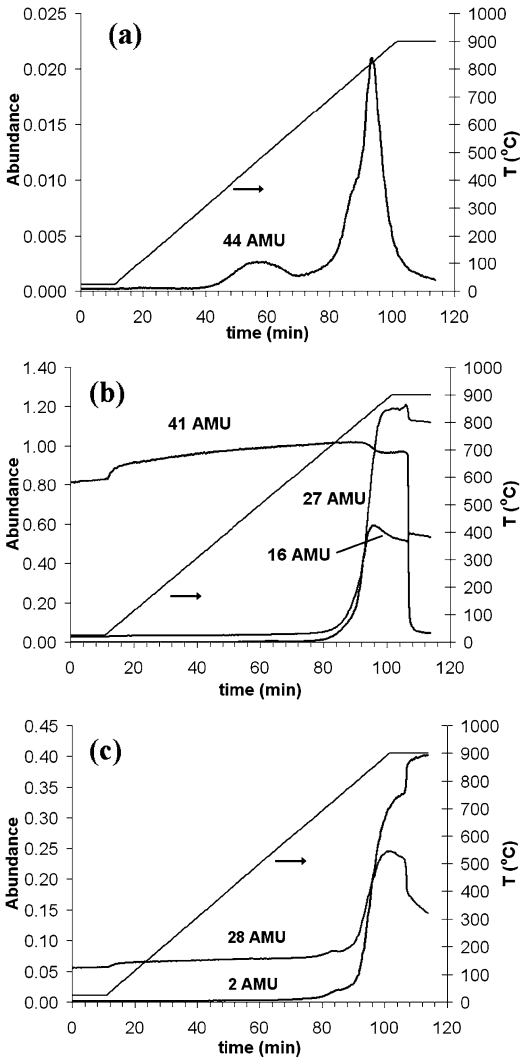

Fig. 1. Major products formed during acetonitrile pyrolysis over silica detected by MS; shown are the main ion fragments for (a) CO_2, (b) CH_3CN, HCN, and CH_4, and (c) N_2 and H_2.

cyanide (HCN), methane (CH_4), molecular nitrogen, and molecular hydrogen, as shown in Figs. 1b and 1c. Quantification of the products based on the total ion count for each species taking into account ionization probabilities provided by the mass spectrometer manufacturer revealed that at 900 °C, on average over all of the samples, 0.48 mol HCN, 0.35 mol CH_4, 0.10 mol N_2, and 0.53 mol H_2 were produced for each mol of acetonitrile (CH_3CN) sent to the furnace. There was very little difference in these values for the samples tested, with standard deviations <10%. Based on molar balances, the species not detected by the mass spectrometer comprised approximately 1.17 mol of C, 0.32 mol of N, and 0.06 mol of H per mol of acetonitrile fed. Both solid carbon, which deposits on the support, and tar, which deposits at the furnace exit, accounted for the products not detected by the mass spectrometer.

3.2. Sample preparation

A wide range of conditions were used for the pyrolysis of acetonitrile. Table 1 gives an overview of all of the samples pre-

Table 1
Samples prepared from the pyrolysis of acetonitrile over a support

Support	Metal loading	CH_3CN pyrolysis conditions	Pyrolysis mass gain	Wash conditions	Post wash mass remaining	BET surface area (m^2/g)
SiO_2	None	550 °C, 4 h	1.7%	KOH, HCl	N.A.	N.A.
SiO_2	2% Fe	550 °C, 4 h	3.0%	KOH, HCl	N.A.	N.A.
SiO_2	2% Co	550 °C, 4 h	2.4%	KOH, HCl	1%	N.A.
SiO_2	None	900 °C, 2 h	13.0%	KOH, HCl	20%	288
SiO_2	2% Fe	900 °C, 2 h	18.9%	KOH, HCl	25%	255
SiO_2	2% Co	900 °C, 2 h	13.6%	KOH, HCl	19%	465
SiO_2	2% Co	900 °C, 2 h	13.6%	HF	9%	N.A.
SiO_2	10% Co	900 °C, 2 h	18.8%	KOH, HCl	22%	214
SiO_2	2% Ni	900 °C, 2 h	5.8%	KOH, HCl	9%	N.A.
MgO	None	900 °C, 2 h	4.5%	HCl	22%	181
MgO	2% Fe	900 °C, 2 h	21.9%	HCl	22%	218
MgO	2% Co	900 °C, 2 h	17.7%	HCl	17%	278
MgO	2% Ni	900 °C, 2 h	43.2%	HCl	24%	128
MgO-HSA	None	900 °C, 2 h	5.9%	HCl	25%	256
MgO-HSA	2% Fe	900 °C, 2 h	28.7%	HCl	28%	241

pared, the amount of mass gained during the pyrolysis, the conditions used to wash the carbon product, the mass of product remaining after this wash, and, if sufficient sample was available, the BET surface area. Temperatures as low as 500 °C are reasonable for nanofiber growth from a carbon source [33]; however, a temperature this low is apparently insufficient for the decomposition of acetonitrile. At 900 °C, a better deposition rate was obtained over all of the supports tested. The MgO-supported samples generally had higher deposition rates than the SiO_2-supported samples. The mass gains were similar to the mass gained using alumina-supported particles reported previously [5]. The results of acetonitrile deposition in the absence of a support or in the presence of unsupported metal particles were also reported previously [3].

Based on the amount of mass lost during the washing step, the respective washing techniques effectively removed most of the support. The percentage of mass loss was calculated on the basis of the weight before the wash but after the carbon treatment. The respective washing techniques easily dissolved untreated supports in trial runs; however, it is possible for metal particles and even the metal oxide support particles to become encased by carbon during the pyrolysis, making them impossible to remove during the wash. Thus, not all of the support is removed during the wash. In one instance, for 2% Co/SiO_2, the carbon product was washed with HF acid to compare the effectiveness of the washing procedures. The mass remained after washing with HF acid was smaller than that of KOH and HCl. Further characterization performed to assess the extent of the support removal is discussed in the following sections.

3.3. N_2 physisorption analysis

The surface area of the final carbon material obtained (see Table 1) was much higher than the original support in all cases. Using higher-surface area MgO (150 vs 55 m^2/g) resulted in an only modest increase in surface area of the carbon produced. In general, the surface areas obtained were not as high as those obtained from HF-washed acetonitrile char deposited on alumina [5].

The effect of washing on the pore structure of the samples is apparent from the representative pore size distribution (PSD) plots in Fig. 2. For the SiO_2-supported samples, there was little difference between untreated SiO_2 and the treated samples. Washing the samples opened smaller pores and reduced the larger pores, although a significant portion of larger pores remained. There was a spike in the distribution at 4 nm, which has been observed in samples containing nanofibers [3,5]. As discussed previously, this feature is characteristic of nanostructures, but in reality the distribution may not be so narrow. The other washed SiO_2-supported samples that contained metal had similar distributions, whereas the treated and washed pure SiO_2-supported sample was similar in the larger pore diameter region but did not have a pronounced spike at 4 nm in the smaller pore diameter region (data not shown).

The pore distributions for the MgO-supported samples behaved somewhat differently than those for the SiO_2-supported samples. The addition of metal to MgO and treatment in an acetonitrile atmosphere at 900 °C for 2 h reduced the pore volume drastically (see Fig. 2b). Washing the samples greatly increased the pore volume for both large and small pores, as shown for the carbon derived from 2% Fe/MgO. Again, the characteristic peak at 4 nm was present in all samples; however, it was smallest in the sample that did not contain metal (see Figs. 2b and 2c). It should also be noted that the treated and washed Ni/MgO sample had considerably less pore volume in the larger pore diameter region compared with the other samples (data not shown).

3.4. XRD

XRD patterns demonstrate the effectiveness of washing samples and also provide information about other phases present and the crystalline properties of the carbon. Fig. 3 compares the diffraction pattern of treated but unwashed Fe/MgO with those of the washed carbon samples derived from MgO-based supports. The pattern for the unwashed sample clearly shows that the MgO phase was highly crystalline, because the only peaks present were from cubic MgO. In the pure MgO-supported

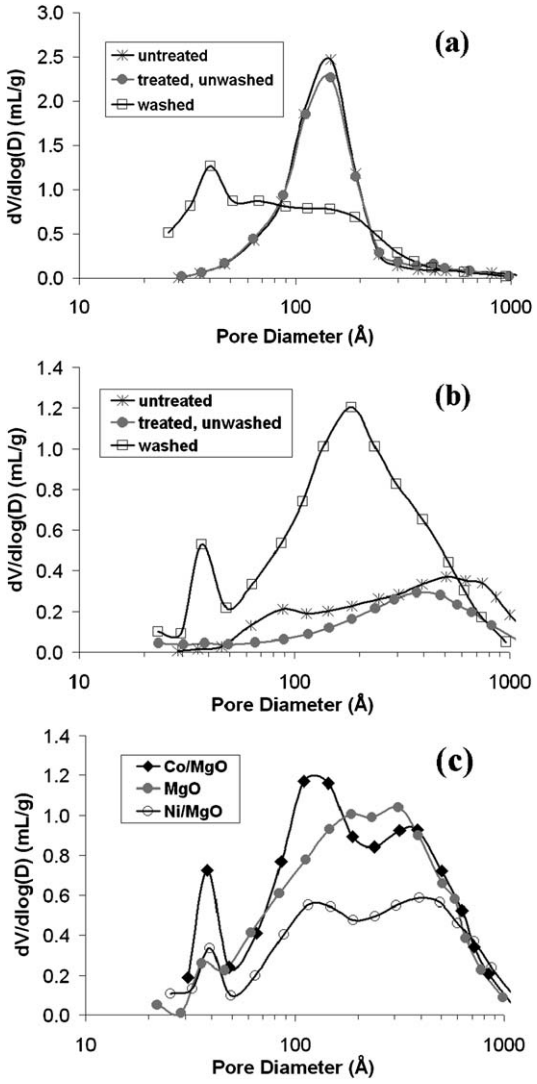

Fig. 2. PSD analysis showing samples throughout there preparation process (treatments were carried out at 900 °C) for (a) Co/SiO_2, (b) Fe/MgO, and (c) other treated and washed magnesia-based samples shown for comparison.

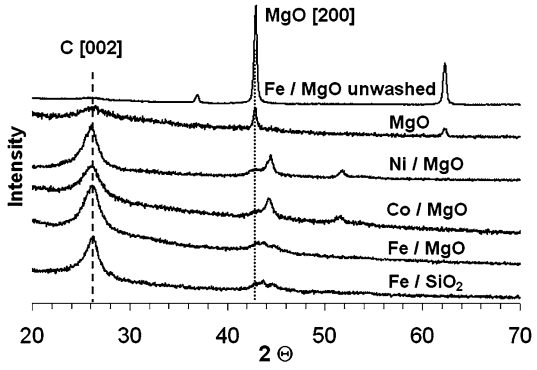

Fig. 3. XRD patterns of CN_x samples prepared from acetonitrile pyrolysis over various supports at 900 °C (samples were washed unless otherwise noted).

sample, a small amount of MgO was still apparent even after the wash, but for the metal-containing samples, all of the detectable MgO was removed. The only peaks remaining can be attributed to poorly crystalline graphitic carbon, with the main peak being C [002], and various phases of the metal (peaks between 42° and 46° 2Θ). Characterization of the metal phases by Mössbauer and X-ray absorption spectroscopy will be presented elsewhere, but for similar materials, carbide, metallic, and oxide phases are typically observed. The presence of these metal species in acetonitrile-treated iron particles (along with their XRD patterns) has been reported elsewhere [34–36]. The only major differences in the samples derived from various metal particles are in the patterns attributed to the metal phases. Fig. 3 also shows the pattern for the carbon derived from 2% Fe/SiO_2. The diffraction pattern is nearly identical to the pattern for the carbon obtained from 2% Fe/MgO. Because the SiO_2 is not crystalline, patterns of the unwashed samples resembled diluted versions of the washed samples; thus these patterns are not shown.

3.5. TPO

The nitrogen-containing carbon materials obtained after the washing step were characterized by TPO with in situ TGA-DSC and gaseous product analysis with a mass spectrometer. These experiments serve several functions. First, the amounts of noncombustibles in the samples can be determined from the gravimetric analysis, indicating how much of the metal catalyst or inorganic precursor remains entrapped in the sample after the wash. Second, the amount of nitrogen in the sample can be estimated based on the amount of carbon oxides and nitrogen oxides released during the combustion and detected with the mass spectrometer. Third, from the combination of all of the signals followed in TPO, the nature of the carbon can be characterized based on its ease of oxidation.

The signals from a typical analysis are displayed in Fig. 4 for the sample prepared from Fe/MgO-(HSA). The exothermic DSC signal began to become positive at around 300 °C, indicating the onset of oxidation. Significant oxidation did not occur until above 400 °C, at which point the TG signal decreased. The derivative of the TG signal (shown in Fig. 4b) exactly mirrored the DSC signal, as expected. This sample had two separate oxidation peaks. All of the samples containing metal had multiple oxidation peaks, whereas the samples prepared on metal-free supports contained only one oxidation peak, similar to pure acetonitrile char [3] or acetonitrile char deposited on alumina [5]. It is not clear whether the multiple peaks originated from multiple types of carbon or were caused by metal particles in contact with carbon, thus catalyzing combustion of that carbon. The next paper in this series will compare TPO profiles with surface properties and oxygen activation activity. The sample shown in Fig. 4 lost 92% of its mass, as is apparent from the TG signal; thus, it still contained some noncombustible inorganic material even after washing with HCl.

The products of combustion were monitored with a mass spectrometer. Only CO_2 formed in the excess oxygen environment, although small amounts of CO would be difficult to differentiate from the fragment at 28 AMU for CO_2, which had an intensity of 12% of the 44-AMU signal. As Fig. 4 shows, the 44-AMU signal matched the DSC signal. In addition, NO was detected as a product of combustion, with the main frag-

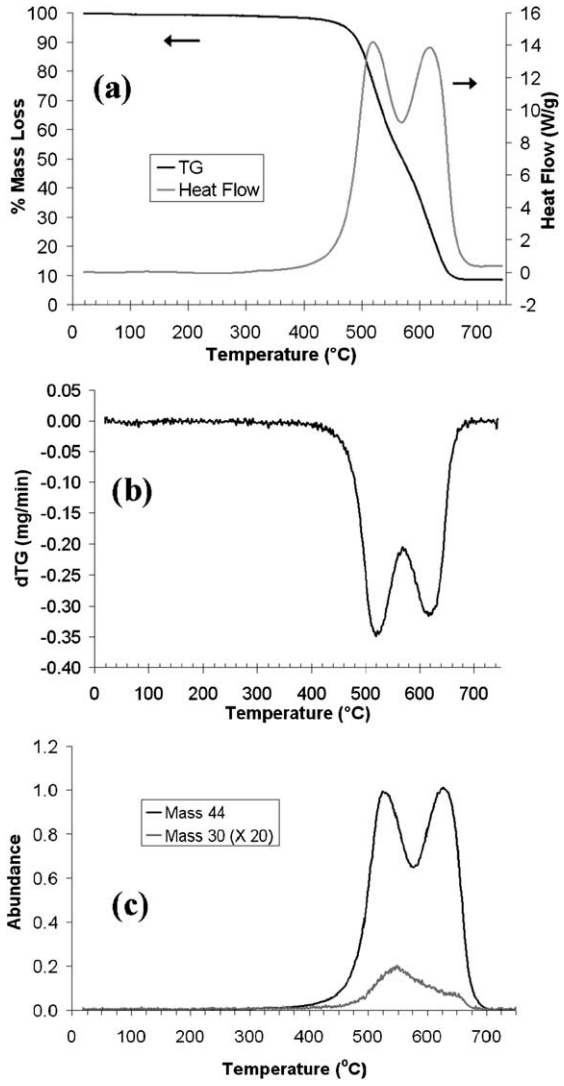

Fig. 4. TPO analysis of washed carbon prepared from acetonitrile pyrolysis over 2% Fe/MgO; (a) thermogravimetric and calorimetry signals, (b) derivative of the TG signal, and (c) major oxidation products detected by the mass spectrometer.

ment at 30 AMU. NO production did not follow CO_2 production in every sample; for instance, Fig. 4 shows that more NO was produced during the first oxidation peak. In the samples without metal particles, NO release was consistently heavier at the end of the combustion. The samples containing metal typically released more NO early in combustion, similar to Fe/MgO-(HSA). Previously we reported that for carbon formed on alumina supports from acetonitrile pyrolysis, NO and CO_2 production followed each other [5]. However, these TPO experiments were carried out under different conditions, and the multiple combustion peaks in the TPO of the alumina samples were not as well defined.

It should be mentioned that NO_2 did not appear to form from CN_x combustion. For all of the samples, the 46-AMU signal was much smaller than the 30-AMU signal (generally about 1/0th the size) and had the same shape as the 44-AMU signal; thus, the 46-AMU signal was likely just a contribution from CO_2. In previous work, in which TPO was conducted with a plug-flow setup and the mass spectrometer was immediately attached at the exit, also found no NO_2 [5]. Montoya et al. modeled the formation of NO during CN_x combustion and found it to be an energetically favorable process [37]. Considering the high temperatures at which the NO signal was observed, NO_2 formation from NO oxidation would be thermodynamically limited under these conditions.

Table 2
Results of oxidation analysis for washed CN_x samples prepared from CH_3CN pyrolysis at 900 °C for 2 h

Support	Metal loading	Wash conditions	% of mass combusted	% nitrogen
SiO_2	None	KOH, HCl	61%	1.1%
SiO_2	2% Fe	KOH, HCl	83%	0.8%
SiO_2	2% Co	KOH, HCl	60%	2.9%
SiO_2	2% Co	HF	72%	2.9%
SiO_2	10% Co	KOH, HCl	44%	2.1%
SiO_2	2% Ni	KOH, HCl	49%	1.5%
MgO	None	HCl	81%	1.6%
MgO	2% Fe	HCl	93%	0.9%
MgO	2% Co	HCl	86%	1.5%
MgO	2% Ni	HCl	90%	0.9%
MgO-HSA	None	HCl	87%	1.4%
MgO-HSA	2% Fe	HCl	92%	0.7%

Using a standard mixture of NO and CO_2, the MS response was calibrated; therefore, the relative intensities of the 30- and 44-AMU signals could be used to quantify the amount of carbon and nitrogen in the samples. Table 2 reports the results from this analysis, as well as the total mass loss for all of the samples tested. Two trends in this data are noteworthy. First, from the mass lost, it is apparent that removing SiO_2 was more difficult than removing MgO. Even if a SiO_2-supported sample were washed with concentrated HF acid, the percentage of combustion (i.e., mass loss) would be lower than that for any of the MgO-supported samples. This seems to indicate that a significant portion of SiO_2 is protected by carbon from the washing. Second, the mass spectrometer signal integrations clearly show that the samples had varying nitrogen content. In particular, the Co/SiO_2-supported samples produced carbon that contains more nitrogen than the other samples. Because nitrogen content does not increase with Co loading, it is unlikely that the additional NO produced in this sample originated from cobalt nitride. The Fe-containing samples consistently have the least amount of nitrogen. In the next paper of this series, we will show that XPS analysis of the same samples detects more nitrogen than TPO, perhaps because the surface is enriched with nitrogen.

3.6. TEM

Electron microscopy imaging confirmed that nanofibers formed during acetonitrile pyrolysis over most of the supports examined. However, unlike pure alumina, which catalyzed the growth of some fiber structures during acetonitrile pyrolysis, the pure SiO_2 and pure MgO samples did not lead to the formation of any fibers. There was no strong evidence that reduction of SiO_2 or MgO occurred during TPAP experiments, unlike in

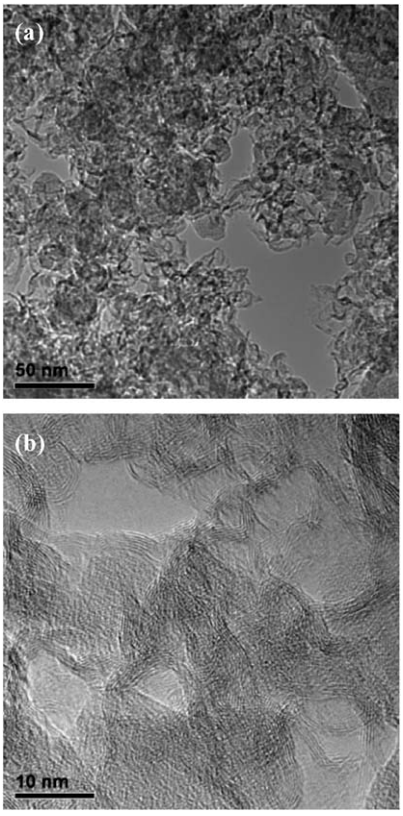

Fig. 5. TEM images of washed acetonitrile char formed on pure SiO_2.

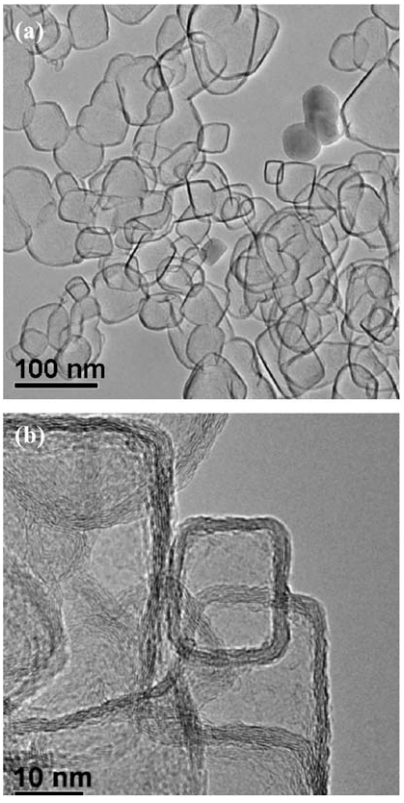

Fig. 6. TEM images of washed acetonitrile char formed on pure MgO.

the alumina experiments reported previously [5]. Images of the carbon deposited on the SiO_2 support (see Fig. 5) showed that the sample contained short strands of graphitic carbon often layered on amorphous particles of silica. Amorphous carbon particles were also present throughout the sample. The carbon deposited on the MgO maintained much better structure after washing. Fig. 6 shows the hollow cubes of nitrogen-containing carbon that remained after MgO crystals were removed. In some cases, the MgO remained inside of the carbon after the wash, as indicated by the dark solid particles in Fig. 6a.

The metal-doped supports all catalyzed fiber formation during pyrolysis. Distributions of the fiber diameters are shown in Fig. 7 for all of the samples, except for Ni/SiO_2, which contained very few fiber structures. The silica-supported Fe and Co CN_x samples formed fibers with average diameter of 62 and 36 nm, respectively. The distribution was much more broad for the Fe sample, as Fig. 7a shows. For the MgO-derived CN_x fibers, the diameter distributions were similar to one another, with the exception of the Ni/MgO sample (see Fig. 7b). The average diameters for the fibers formed from 2% Co/MgO, 2% Fe/MgO, and 2% Fe/MgO-HSA were 32, 36, and 42 nm, respectively. The Ni/MgO formed fibers with an average diameter of 59 nm.

Some typical images of fibers grown from silica-supported and magnesia-supported metals are shown in Figs. 8 and 9, respectively. Most of the Fe- and Co-grown fibers for both the SiO_2 and MgO supports were compartmentalized and stacked together like a stack of cups. This is the same type of structure that formed under similar pyrolysis conditions over Fe/Al_2O_3.

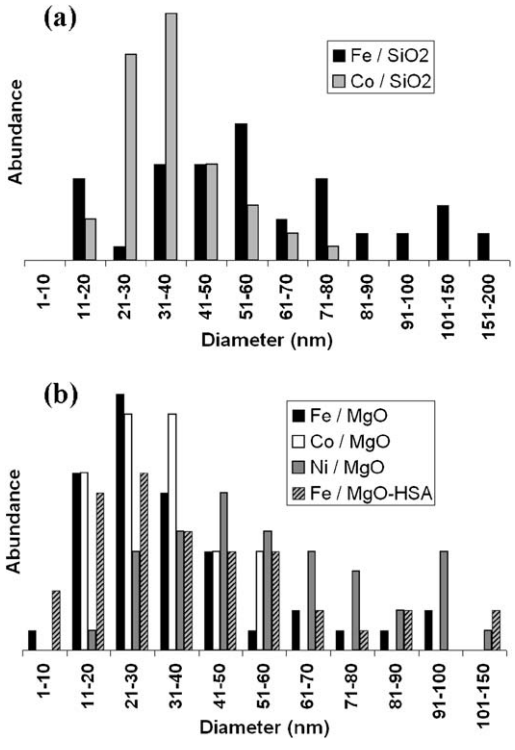

Fig. 7. Diameter distributions for CN_x fibers grown from different metal particles and supports. Distributions were obtained from TEM images.

Multiwalled nanotubes and solid fibers were also found in all of the Fe and Co samples, but to a lesser extent. For the Ni/SiO_2-supported sample, only a small amount of short fiber structures

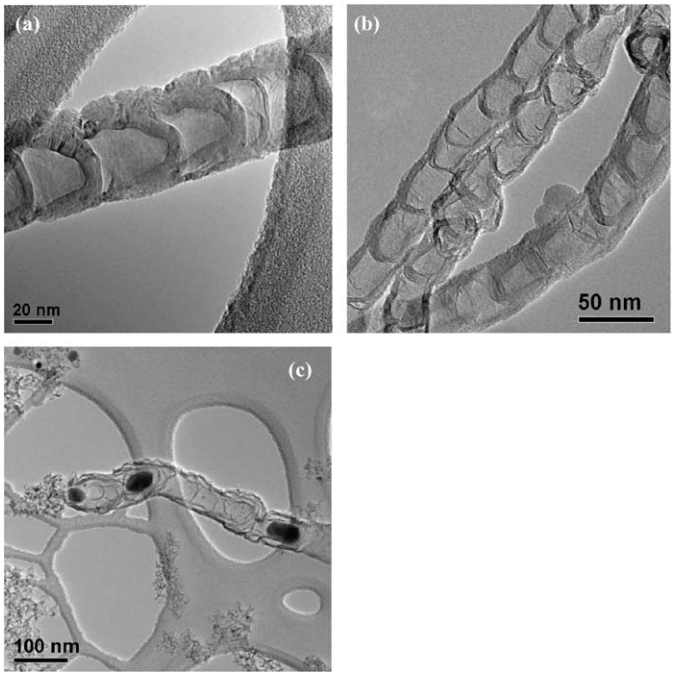

Fig. 8. TEM images of CN_x fibers formed during acetonitrile pyrolysis at 900 °C over (a) 2% Fe/SiO_2, (b) 2% Co/SiO_2, and (c) 2% Ni/SiO_2.

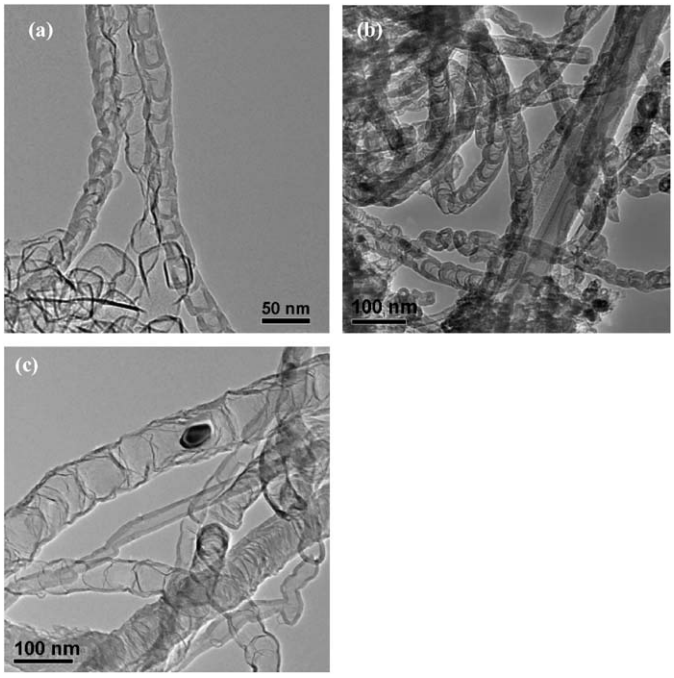

Fig. 9. TEM images of CN_x fibers formed during acetonitrile pyrolysis at 900 °C over (a) 2% Fe/MgO, (b) 2% Co/MgO, and (c) 2% Ni/MgO.

was formed, such as that shown in Fig. 8c. These fibers contained a relatively high amount of large metal particles encased inside of them. The structure of these fibers was hollow, with sporadic and disordered carbon planes inside the fiber. Similarly structured fibers were reported from the same pyrolysis conditions over Ni/Al_2O_3. With Ni/MgO, the same broken multiwalled nanotubes formed along with conventional multiwalled nanotubes and solid fibers.

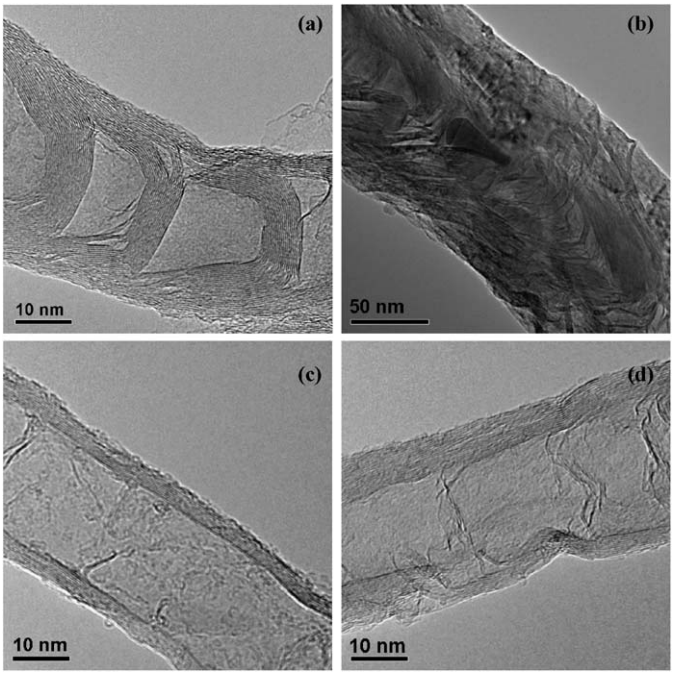

Fig. 10. TEM images representative of particle structures for (a) stacked cups formed on Fe/MgO, (b) solid CN_x fiber grown from Fe/SiO_2, (c) MWNT grown from Fe/MgO, and (d) broken MWNT formed from Fe/MgO.

Table 3
Distribution of CN_x fiber types for samples prepared from acetonitrile pyrolysis at 900 °C

CN_x precursor	Percentage of particular fiber type			
	Stacked cups	Fibers	MWNTs	Broken MWNTs
Fe/Al_2O_3	57%	3%	40%	0%
Ni/Al_2O_3	6%	17%	17%	60%
Fe/SiO_2	71%	7%	18%	4%
Co/SiO_2	66%	0%	13%	21%
Fe/MgO	42%	14%	9%	35%
Co/MgO	54%	10%	21%	15%
Ni/MgO	13%	25%	18%	45%
Fe/MgO-HSA	60%	10%	20%	10%

Although the figures in this section show representative images of fibers that formed during acetonitrile pyrolysis over the respective supports, it should be mentioned that the various types of fibers discussed could be found in almost any of the samples. Thus, distributions of the different fiber types within the samples were obtained using TEM. The four major types of fibers observed were defined as stacked cups (see Figs. 8a and 8b, 9a and 9b, and 10a), solid fibers (see Fig. 10b), MWNTs (see Fig. 10c), and broken MWNTs (see Figs. 8c, 9c, and 10d). Some fiber structures were ambiguous and counted half toward two different fiber types. The distribution of all fiber-containing samples, given in Table 3, shows roughly to what extent the various fiber types were found in each sample. Clearly, Fe- and Co-derived samples preferentially catalyzed the formation of stacked-cup fibers, whereas Ni samples favored the broken MWNTs, regardless of the support. In general, the only trend with respect to fiber type and fiber diameter was that solid fibers always had very large relative diameters compared with other

fibers in the samples, whereas MWNTs typically had smaller diameters.

4. Conclusions

Nitrogen-containing carbon nanostructures were prepared from the decomposition of acetonitrile at 900 °C over silica and magnesia supports. For the carbon grown from supported Fe and Co particles, compartmentalized fibers with a stacked-cup structure predominantly formed, whereas mostly broken multiwalled nanotubes formed from Ni particles. These observations are consistent with the structures formed from alumina-supported Fe and Ni. The diameter of the fibers varied significantly depending on the support used, and the total nitrogen content varied depending on the metal–support combination used. Washing the silica-derived samples removed some of the silica, but based on TPO/TGA results, about half of the sample still consisted of silica. This was most likely caused by the complete encapsulation of silica particles in carbon, because washing with HF acid yielded only a slight improvement. Conversely, the magnesia particles could be easily removed by washing with HCl acid, leaving behind only carbon and encapsulated metal particles. All of the samples had high surface areas after washing.

The stacked-cup-structured fibers formed from Fe and Co particles should have significant edge-plane exposure, which is useful for such applications as catalysis. The next paper of this series will investigate the surface and electrochemical properties of the nitrogen-doped carbon, with specific focus on catalytic activity for the oxygen reduction reaction.

Acknowledgments

The authors gratefully acknowledge the financial support provided for this work by the National Science Foundation (grants NSF-CTS-0437451 and NSF-DGE-0221678) and by the Ohio Department of Development through the Wright Center of Innovation Program.

References

[1] V.V. Strelko, V.S. Kuts, P.A. Thrower, Carbon 38 (2000) 1499–1525.
[2] K. Kinoshita, Carbon, Electrochemical and Physicochemical Properties, Wiley–Interscience, New York, 1988.
[3] P.H. Matter, L. Zhang, U.S. Ozkan, J. Catal. 239 (2006) 83–96.
[4] P.H. Matter, U.S. Ozkan, Catal. Lett. 109 (2006) 115–123.
[5] P.H. Matter, E. Wang, M. Arias, E.J. Biddinger, U.S. Ozkan, J. Phys. Chem. B (2006), in press.
[6] S. van Dommele, A. Romero-Izquirdo, K.P. de Jong, J.H. Bitter, Proceeding of the 19th NACS Meeting, Philadelphia, PA, 2005.
[7] S. Maldonado, K.J. Stevenson, J. Phys. Chem. B 108 (2004) 11,375–11,383.
[8] S. Maldonado, K.J. Stevenson, J. Phys. Chem. B 109 (2005) 4707–4716.
[9] B.M. Way, J.R. Dahn, J. Electrochem. Soc. 141 (1994) 907.
[10] W. Weydanz, B.M. Way, T. van Buuren, J. Dahn, J. Electrochem. Soc. 141 (1994) 900.
[11] L. Duclaux, E. Frackowiak, F. Beguin, J. Power Sourc. 81–82 (1999) 323–327.
[12] T. Nakajima, M. Koh, M. Takashima, Electrochim. Acta 43 (1998) 883–891.
[13] A.-C. Dupuis, Progress Mater. Sci. 50 (2005) 929–961.
[14] T. Nakajima, M. Koh, Carbon 35 (1997) 203.
[15] S.Y. Brichka, G.P. Prikhod'ko, A.V. Brichka, V.M. Ogenko, A.A. Chuiko, Theor. Exp. Chem. 38 (2002) 114–117.
[16] Y. Hao, L. Qingwen, Z. Jin, L. Zhongfan, Chem. Phys. Lett. 380 (2003) 347–351.
[17] M. Terrones, A.M. Benito, C. Manteca-Diego, W.K. Hsu, O.I. Osman, J.P. Hare, D.G. Reid, H. Terrones, A.K. Cheetham, K. Prassides, H.W. Kroto, D.R.M. Walton, Chem. Phys. Lett. 257 (2006) 576–582.
[18] M. He, S. Zhou, J. Zhang, Z. Liu, C. Robinson, J. Phys. Chem. B 109 (2005) 9275–9279.
[19] R. Kvon, G. Il'inich, A. Chuvilin, V. Likholobov, J. Molec. Catal. A Chem. 158 (2000) 413.
[20] R. Sen, B.C. Satishkumar, A. Govindaraj, K.R. Harikumar, G. Raina, J.-P. Zhang, A.K. Cheetham, C.N.R. Rao, Chem. Phys. Lett. 287 (1998) 671–676.
[21] R. Sen, B.C. Satishkumar, A. Govindaraj, K.R. Harikumar, M.K. Renganathan, C.N.R. Rao, Mater. Chem. Commun. 7 (1997) 2335–2337.
[22] S. Trasobares, O. Stephan, C. Colliex, W.K. Hsu, H.W. Kroto, D.R.M. Walton, J. Chem. Phys. 116 (2002) 8966–8972.
[23] M. Terrones, P. Redlich, N. Grobert, S. Trasobares, W.-K. Hsu, H. Terrones, Y.-Q. Zhu, J.P. Hare, C.L. Reeves, A.K. Cheetham, M. Rühle, H.W. Kroto, D.R.M. Walton, Adv. Mater. 11 (1999) 655–658.
[24] K. Suenaga, M. Yudasaka, C. Colliex, S. Iijima, Chem. Phys. Lett. 316 (2000) 365–372.
[25] J. Lahaye, G. Nanse, A. Bagreev, V. Strelko, Carbon 37 (1999) 585–590.
[26] S. Maldonado, S. Morin, K.J. Stevenson, Carbon 44 (2006) 1429–1437.
[27] N.M. Rodriguez, A. Chambers, R.T.K. Baker, Langmuir 11 (1995) 3862–3866.
[28] R.T.K. Baker, Carbon 27 (1989) 315–323.
[29] R.T.K. Baker, M.S. Kim, A. Chambers, C. Park, N.M. Rodriguez, Stud. Surf. Sci. Catal. 111 (1997) 99–109.
[30] C.J. Lee, J. Park, J.A. Yu, Chem. Phys. Lett. 360 (2002) 250–255.
[31] A. Kukovecz, Z. Konya, N. Nagaraju, I. Willems, A. Tamasi, A. Fonseca, J.B. Nagy, I. Kiricsi, Phys. Chem. Chem. Phys. 2 (2000) 3071–3076.
[32] C. Park, M.A. Keane, J. Catal. 221 (2004) 386–399.
[33] M. Audier, M. Coulon, Carbon 23 (1985) 317–323.
[34] G. Faubert, R. Cote, D. Guay, J.P. Dodelet, G. Denes, C. Poleunis, P. Bertrand, Electrochim. Acta 43 (1998) 1969.
[35] R. Cote, G. Lalande, D. Guay, J.P. Dodelet, G. Denes, J. Electrochem. Soc. 145 (1998) 2411.
[36] G. Lalande, R. Cote, D. Guay, J.P. Dodelet, L.T. Weng, P. Bertrand, Electrochim. Acta 42 (1997) 1379.
[37] A. Montoya, J. Gil, F. Mondragon, T.N. Truong, Fuel Process. Technol. 77–78 (2002) 453–458.